Superlattices and Microstructures 133 (2019) 106185

Contents lists available at ScienceDirect

Superlattices and Microstructures

journal homepage: www.elsevier.com/locate/yspmi

Strain and electric field engineering of electronic structures and Schottky contact of layered graphene/$Ca(OH)_2$ heterostructure

Chuong V. Nguyen [a], Doan V. Thuan [b], Huynh V. Phuc [c], Bui D. Hoi [d], Nguyen N. Hieu [d], Bin Amin [e], Khang D. Pham [f,g,*]

[a] Department of Materials Science and Engineering, Le Quy Don Technical University, Ha Noi, Viet Nam
[b] NTT Hi-Tech Institute, Nguyen Tat Thanh University, Ho Chi Minh City, Viet Nam
[c] Division of Theoretical Physics, Dong Thap University, Dong Thap, Viet Nam
[d] Institute of Research and Development, Duy Tan University, Da Nang, Viet Nam
[e] Department of Physics, Abbottabad University of Science and Technology, Abbottabad, Pakistan
[f] Laboratory of Applied Physics, Advanced Institute of Materials Science, Ton Duc Thang University, Ho Chi Minh City, Viet Nam
[g] Faculty of Applied Sciences, Ton Duc Thang University, Ho Chi Minh City, Viet Nam

ARTICLE INFO

Keywords:
Graphene
Calcium hydroxide
DFT calculations
Schottky and Ohmic contacts

ABSTRACT

In this work, we propose an ultrathin graphene/$Ca(OH)_2$ van der Waals heterostructure (vdWH) and investigate its structural stability, electronic structures and Schottky contact types modulation by ab initio calculations. Our results show the preservation of graphene and $Ca(OH)_2$ intrinsic electronic properties in graphene/$Ca(OH)_2$ vdWH, which is mainly characterized by the physicoadsorption interaction with the binding energy of -33.37 meV per carbon atom. $Ca(OH)_2$ monolayer stacking on graphene to form the vdWH forms the *p*-type Schottky contact and opens a valuable graphene's band gap of 9.7 meV, suggesting its promising application in high speed nanoelectronic devices. Furthermore, electric field and vertical strain can be used to modulate the Schottky contact from the *p*-type to the *n*-type one and to Ohmic contact. These predictions demonstrate the potential candidate of the G/$Ca(OH)_2$ vdWH for future nanoelectronic applications.

1. Introduction

Today, searching for new materials with appropriate physical properties for high-performance electronic and optoelectronic devices is gaining great attention from the research community. Graphene (G) [1] is recently considered as a promising material for wide range of applications, such as field-effects transistors (FETs) [2,3], photodetectors [4]. However, in its semi-metallic form, the G has limited functionality in the electronic devices and semiconductor technology [5]. Currently, the formation of the vdWHs by placing G above on top of other two-dimensional (2D) semiconducting materials is one of the commonly used strategies to break this limitation of the G. Over the past decade, using this strategy, series G-based vdWHs have been synthesized experimentally and investigated theoretically, such as G/*h*-BN [6–9], G/GaSe [10–13], G/$PtSe_2$ [14–16], G/WSe_2 [17–19], G/phosphorene [20–22], G/MXene [23–25], G/GeC [26] and so on. Aziza and his co-workers [11,12] demonstrated the preservation of the graphene's linear dispersion in G/GaSe vdWH. Sun et al. [17] investigated the structural and electronic properties of the G/WSe_2 vdWH without and with the presence of external conditions. Whereas, Wang et al. [26] constructed a *p*-type Schottky contact of the G/GeC vdWH and demonstrated that controlling the interlayer distance and applying a perpendicular electric field are two promising methods for

* Corresponding author.
E-mail address: phamdinhkhang@tdtu.edu.vn (K.D. Pham).

https://doi.org/10.1016/j.spmi.2019.106185
Received 8 June 2019; Received in revised form 7 July 2019; Accepted 10 July 2019
Available online 15 July 2019

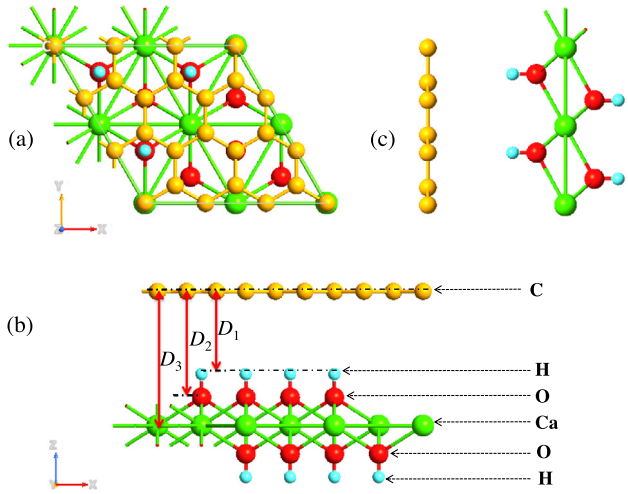

Fig. 1. (a) The top view and (b, c) the side view of the G/$Ca(OH)_2$ vdWH after relaxation.

tuning its electronic properties. All these findings indicate that the G-based vdWHs can potentially be used in future high performance optoelectronic devices.

Recently, a new type of the alkaline-earth-metal hydroxides family, namely Portlandite $Ca(OH)_2$ has been synthesized experimentally from its bulk form [27]. Its structural, electronic, and vibrational properties have also investigated theoretically using DFT method. They predicted that the $Ca(OH)_2$ monolayer is dynamically stable even at high temperatures. It forms a direct band gap semiconductor, which is insensitive to thickness [28]. However, its band gap can be controlled under external conditions, including strain and electric field, that makes $Ca(OH)_2$ material suitable for future electronic application. To date, various vdWHs between $Ca(OH)_2$ monolayer and other 2D materials have been proposed and investigated [29–32]. Torun et al. [32] predicted a type-II staggered gap in GaS/$Ca(OH)_2$ vdWH, whereas, a type-I straddling gap was observed in arsenene/$Ca(OH)_2$ vdWH [29]. All these above findings indicate that the $Ca(OH)_2$ is a promising material, that can be used commonly to combine with other 2D materials. Therefore, in the present work, we first propose an ultrathin vdWH between graphene and $Ca(OH)_2$ monolayer and then consider the electronic structures and Schottky contact type modulation in the formed vdWH using density functional theory (DFT).

2. Computational methods

Our calculated results are performed in the framework of density functional theory (DFT) and the open-source Quantum Espresso package [33]. We opted to choose the generalized gradient approximation (GGA) [34] and the Perdew–Burke–Ernzerhof (PBE) [35] parametrization for describing the exchange and correlation energies. In order to calculate the effect of the physicoadsorption interaction, occurring in layered systems, including graphene-based vdWHs, we used DFT-D2 method [36]. We have previously used this approach to describe successfully the weak vdW interactions in layered graphene-based vdWHs [37,38]. Also, DFT method underestimates the band gaps of semiconductors, but it is good at predicting correct trends and physical mechanisms. Thus, the hybrid Heyd–Scuseria–Ernzerhof (HSE06) functional [39] is also used to obtain the more accurate band gap in some cases. In order to calculate the charge transfers in such G/$Ca(OH)_2$ vdWH, we use a Baders charge analysis [40–43]. The cut-off energy for plane wave is set to be 400 eV and the $9 \times 9 \times 1$ k-point meshes are used. The atomic structures of the G/$Ca(OH)_2$ vdWH are fully relaxed within the convergence of forces and energy of 10^{-3} eV/Å and 10^{-6} eV, respectively. Furthermore, to break the interactions between the neighboring layers we applied a large vacuum thickness of 25 Å along the z direction.

3. Results and discussion

The lattice parameters of the isolated graphene and $Ca(OH)_2$ monolayer are firstly checked and listed in Table 1. It is clear that these values are consistent with previous experimental measurements and theoretical calculations [27]. Therefore, to form the G/$Ca(OH)_2$ vdWH, we opt to use a large supercell of the heterostructure, consisting of (2×2) $Ca(OH)_2$ supercell and (3×3) graphene's supercell. The lattice mismatch of the vdWH is smaller than 3%, which affects insignificantly the main electronic properties of considered here heterostructure. The relaxed geometric structure of the G/$Ca(OH)_2$ vdWH illustrates in Fig. 1. The vertical interlayer distance between graphene layer and the hydrogen, oxygen and calcium layers in the G/$Ca(OH)_2$ vdWH are defined by D_1, D_2 and D_3, which respectively are 2.380 Å, 3.352 Å, and 4.490 Å, as listed in Table 1. To check the stability of such vdWH, we further explore its binding energy, which can be calculated as follows: $E_b = [E_H - E_G - E_{Ca}]/S$, where E_H, E_G, and E_{Ca}, respectively, are the total energies of the vdWH, isolated graphene and $Ca(OH)_2$. S is the surface area of considered vdWH. Our calculated E_b at the equilibrium state is −11.65 meV/Å, as listed in Table 1. Also, such G/$Ca(OH)_2$ vdWH is energetically stable

Table 1
Calculated lattice parameters a (in Å), vertical interlayer distances (in Å), band gap (in eV), binding energy (meV/Å), the nSC-type and pSC-type and the work function (in eV) of all considered here materials.

	a	D_1	D_2	D_3	E_g	E_b	$\Phi_{B,n}$	$\Phi_{B,p}$	W
Graphene	2.46	–	–	–	0	–	–	–	4.25
$Ca(OH)_2$	3.59	–	–	–	3.680	–	–	–	4.78
$G/Ca(OH)_2$	7.18	2.380	3.352	4.490	9.7×10^{-3}	−11.65	2.904	0.780	4.54

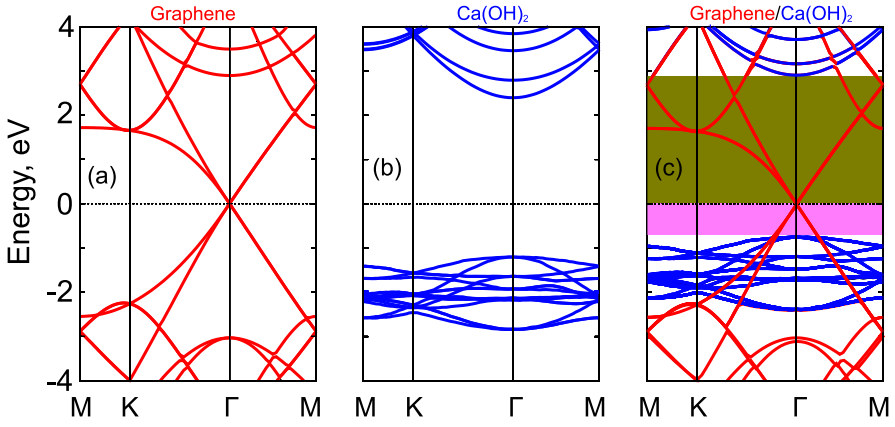

Fig. 2. Projected band structures of (a) (3 × 3) graphene, (b) (2 × 2) $Ca(OH)_2$ and (c) $G/Ca(OH)_2$ vdWH. Contributions from the graphene and $Ca(OH)_2$ layers are highlighted in red and blue lines, respectively.

due to the obtained negative value of E_b. In addition, we find that this value of E_b is comparable with that in other graphene-based vdWHs [22,44–46].

It is clear from Fig. 2(a) that the isolated (3 × 3) graphene shows a gap-less semiconductor with the linear dispersion relation at the Dirac Γ, which is in agreement with other calculations [26,37]. It should be noted here that the linear dispersion relation is shifted from Dirac K point in graphene's unit cell to the Γ point in the (3 × 3) graphene's supercell due to the band folding effect. This trend has also been observed in other graphene-based heterostructures. The band structure of the $Ca(OH)_2$ with a (2 × 2) supercell is shown in Fig. 2(b). It is shown a direct band gap semiconductor. This direct band gap obtained from PBE/HSE calculation is 3.680 eV/5.18 eV which is in close agreement with previous reports [27,29]. Both the topmost valence band (VBM) and the bottom conduction band (CBM) of the $Ca(OH)_2$ are located at the Γ point. In order to have a better understanding the electronic properties of $G/Ca(OH)_2$ vdWH, we present its projected band structure in Fig. 2(c). We find that the band structure of $G/Ca(OH)_2$ vdWH seems to be simple sum of each component. It indicates that the band structures of graphene and $Ca(OH)_2$ are well preserved in vdWH. Thus, their key intrinsic properties can be maintained in such vdWH. More interestingly, when we find that the formation of the $G/Ca(OH)_2$ vdWH tends to open a tiny band gap of 9.7 meV around the Fermi level of graphene, making it acceptable for high speed electronic devices.

Now a question is whether a high carrier mobility of perfect graphene can be maintained in the $G/Ca(OH)_2$ vdWH. Thus, we further calculate the effective masses for electrons (m_e^*) and for holes (m_h^*) of the $G/Ca(OH)_2$ vdWH. It is clear that the effective masses m_e^* and m_h^* of the $G/Ca(OH)_2$ vdWH are closely related to its carrier mobility, which can be calculates as follows: $\mu = e\tau/m^*$. The m_e^* and m_h^* of the $G/Ca(OH)_2$ vdWH are calculated by fitting parabolic functions to the CBM and VBM of the $G/Ca(OH)_2$ vdWH around the Fermi level at the Dirac Γ point, that is:

$$\frac{1}{m^*} = \frac{1}{\hbar}\frac{\partial^2 E(k)}{\partial k^2} \tag{1}$$

where $\hbar$ and k, respectively, are the wave vector and the Planck's constant. Our calculated effective masses m_e^* and m_h^* are calculated to be $2.43 \times 10^{-3}\ m_0$ and $1.32 \times 10^{-3}\ m_0$, respectively, which are comparable with those in perfect graphene. It demonstrates the $G/Ca(OH)_2$ vdWH has a high carrier mobility and thus becomes a suitable material for designing high speed field effect transistors.

Furthermore, when placing graphene on the $Ca(OH)_2$ monolayer to form $G/Ca(OH)_2$ vdWH, it represents a metal/semiconductor contact, in which two different types of Schottky contact type(SC-type) or Ohmic contact type (OC-type) can be formed. It is obvious from Fig. 2(c) that the Fermi level lies between the VBM and CBM of the $Ca(OH)_2$ semiconductor. Thus, the SC-type is formed in such $G/Ca(OH)_2$ vdWH. The n-type and p-type Schottky barriers (SB) can be calculated according to the Schottky–Mott rule [47], that is $\Phi_{B,n} = E_{CBM} - E_F$ and $\Phi_{B,p} = E_F - E_{VBM}$, where E_{CBM}, E_F and E_{VBM}, respectively, are the CBM at Γ point, the Fermi level, and the VBM at Γ point. Our calculated $\Phi_{B,n}$ and $\Phi_{B,p}$ are 2.904 eV and 0.780 eV, respectively, as listed in Table 1. It suggests that the Fermi level is closer to the VBM than to the CBM of the $Ca(OH)_2$, indicating that the $G/Ca(OH)_2$ vdWH forms the pSC-type with a small SB of $\Phi_{B,p} = 0.78$ eV.

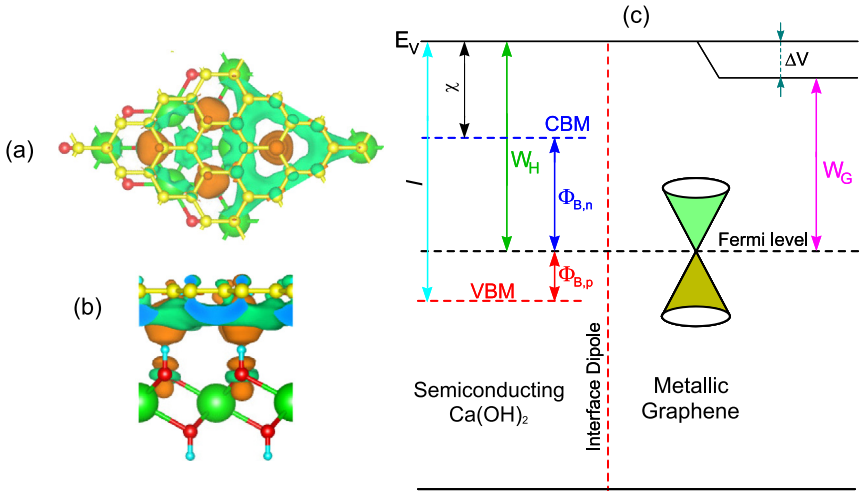

Fig. 3. (a) Top view and (b) side view of the charge density difference in the G/$Ca(OH)_2$ vdWH. (c) The schematic model of the band alignment in the G/$Ca(OH)_2$ vdWH.

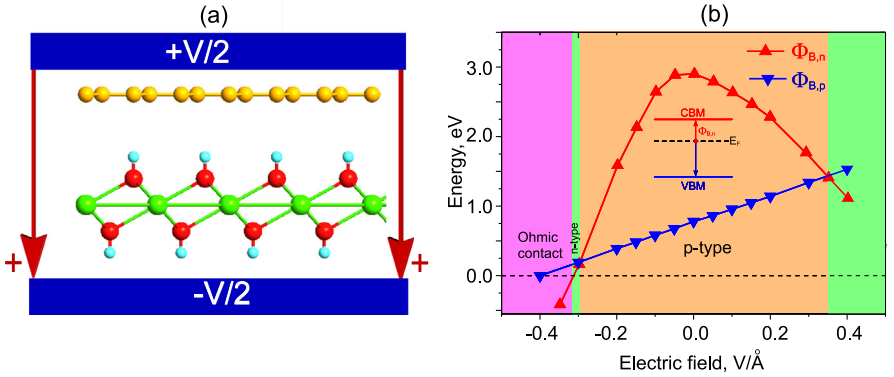

Fig. 4. (a) Schematic model of an applied electric field perpendicular to the heterostructure surface along the z direction of the G/$Ca(OH)_2$ vdWH. The electric field, pointing from the graphene to the $Ca(OH)_2$ layer is defined as the positive direction. (b) The variation of the nSC-type and pSC-type of G/$Ca(OH)_2$ vdWH under electric field. The magenta, green and orange regions represent the Ohmic contact, the nSC-type and the pSC-type, respectively.

To clearly understand the weak interactions and the charge transfer in the G/$Ca(OH)_2$ vdWH, we further calculate the charge density difference (CDD) as: $\Delta\rho = \rho_H - \rho_G - \rho_{Ca}$, where ρ_H, ρ_G, and ρ_{Ca}, respectively, are the charge densities of such vdWH, the isolated graphene and $Ca(OH)_2$ monolayer. The CDD in such vdWH is plotted in Fig. 3(a,b), which demonstrates the charge transference from the graphene layer to the $Ca(OH)_2$ layer. The green and orange regions represent electrons depletion and accumulation, respectively. It can be seen that there is a tiny charge accumulation around the $Ca(OH)_2$ layer, whereas the charge depletion around the graphene layer. By Bader charge transfer analysis, we find that at the equilibrium state, only 0.004 electrons are transferred from graphene to the $Ca(OH)_2$ layer in such vdWH. Although this charge transfer is weak, it creates an interface dipole and an accompanying potential step (ΔV), as shown in Fig. 3(c). The interface potential step ΔV can be defined as $\Delta V = W_H - W_G$, where W_H and W_G are the work functions of the graphene and its vdWH, respectively. The work functions of the G/$Ca(OH)_2$ vdWH and the isolated graphene are 4.54 eV and 4.25 eV, respectively, as listed in Table 1. When an interface dipole is considered, the nSC-type and pSC-type Schottky barriers can be rewritten as follows:

$$\Phi_{B,n} = W_G + \Delta V - \chi \tag{2}$$

and

$$\Phi_{B,p} = I - W_G - \Delta V \tag{3}$$

where χ and I are the electron affinity and the ionization potential of the $Ca(OH)_2$ semiconductor, respectively.

When using G/$Ca(OH)_2$ vdWH as a component for high-performance nanodevices, it always subjected to electric field ($E_\perp$), which can lead to change in electronic characteristics of vdWH. Thus, it is important to study the effect of $E_\perp$ on the electronic properties of the G/$Ca(OH)_2$ vdWH. The $E_\perp$, pointing from the graphene layer to the $Ca(OH)_2$ layer is defined as the positive

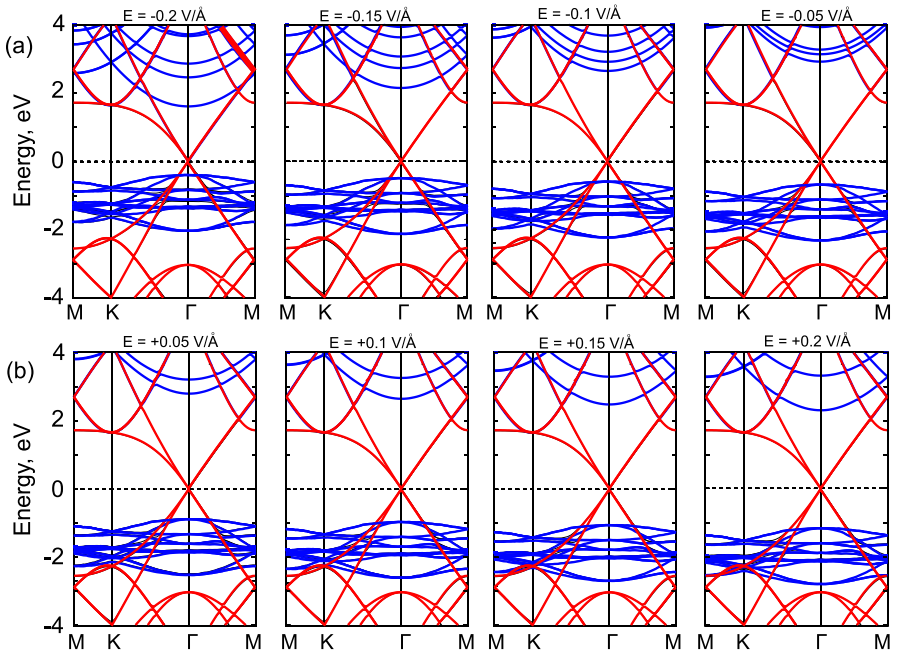

Fig. 5. Projected electronic band structures of the G/Ca(OH)$_2$ vdWH by applying (a) negative $E_\perp$ ranging from −0.2 V/Å to −0.15 V/Å to −0.1 V/Å and −0.05 V/Å and (b) positive $E_\perp$ ranging from +0.05 V/Å, +0.1 V/Å, +0.15 V/Å and +0.2 V/Å.

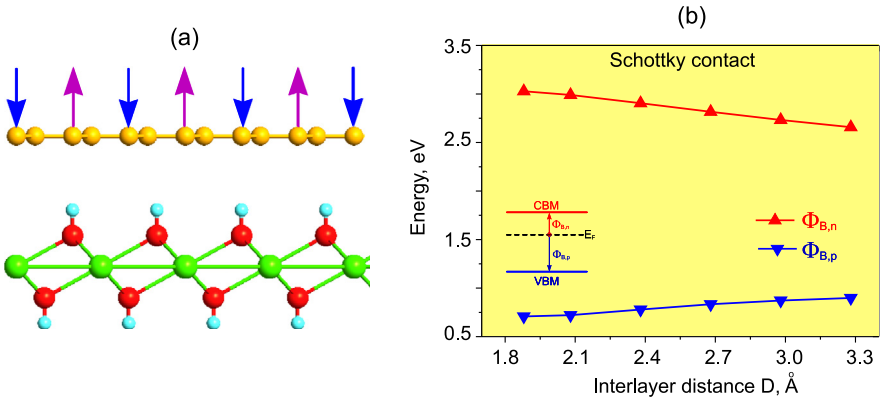

Fig. 6. (a) Schematic model of the vertical (out-of plane) strain by decreasing (green arrows) and increasing (purple arrows) the interlayer distance D_1 of the G/Ca(OH)$_2$ vdWH. (b) The variation of the $\Phi_{B,n}$ and $\Phi_{B,p}$ of the G/Ca(OH)$_2$ vdWH as a function of the interlayer distance D_1.

direction, as illustrated in Fig. 4(a). The variation of the Schottky barriers as a function of the $E_\perp$, applying along the z direction of the G/Ca(OH)$_2$ vdWH is displayed in Fig. 4(b). When a negative $E_\perp$ is applied, we find that the both the $\Phi_{B,n}$ and $\Phi_{B,p}$ linearly decrease with decreasing the strength of the negative $E_\perp$. It can be seen that the $\Phi_{B,n}$ is more sensitive to the negative $E_\perp$ than the $\Phi_{B,p}$. Thus, when the negative $E_\perp$ is applied to the vdWH, the $\Phi_{B,n}$ is reduces faster than the $\Phi_{B,p}$. When the applied negative $E_\perp$ = −0.3 V/Å, the $\Phi_{B,n}$ reduces to 0.22 eV, which is smaller than the $\Phi_{B,p}$ = 0.23 eV. It indicates a transition from the *p*SC-type to the *n*SC-type. When the applied $E_\perp$ is larger than −0.3 V/Å, the $\Phi_{B,n}$ decreases and becomes a negative value, indicating a transformation from the *n*SC-type to the OC-type. The band structures of the G/Ca(OH)$_2$ vdWH under different strengths of the applied negative $E_\perp$ are plotted in Fig. 5(a-d). It can be seen that the VBM of the Ca(OH)$_2$ part of the G/Ca(OH)$_2$ vdWH shifts upwards to the Fermi level with increasing the strength of the negative $E_\perp$, whereas its CBM moves downwards to the Fermi level. It suggests that both the $\Phi_{B,n}$ and $\Phi_{B,p}$ reduce with increasing the negative $E_\perp$. When an applied negative $E_\perp$ is larger than −0.3 V/Å, the VBM of the Ca(OH)$_2$ part moves upwards and crosses the Fermi level, indicating a transformation from the Schottky to the Ohmic contact in the G/Ca(OH)$_2$ vdWH.

When a positive $E_\perp$ is subjected to the G/Ca(OH)$_2$ vdWH, from Fig. 4(b) the gradual decrease in the $\Phi_{B,n}$ with increasing the strength of the positive $E_\perp$ from 0 V/Å to 0.4 V/Å. Quite the contrary, the $\Phi_{B,p}$ linearly increases with increasing the positive electric

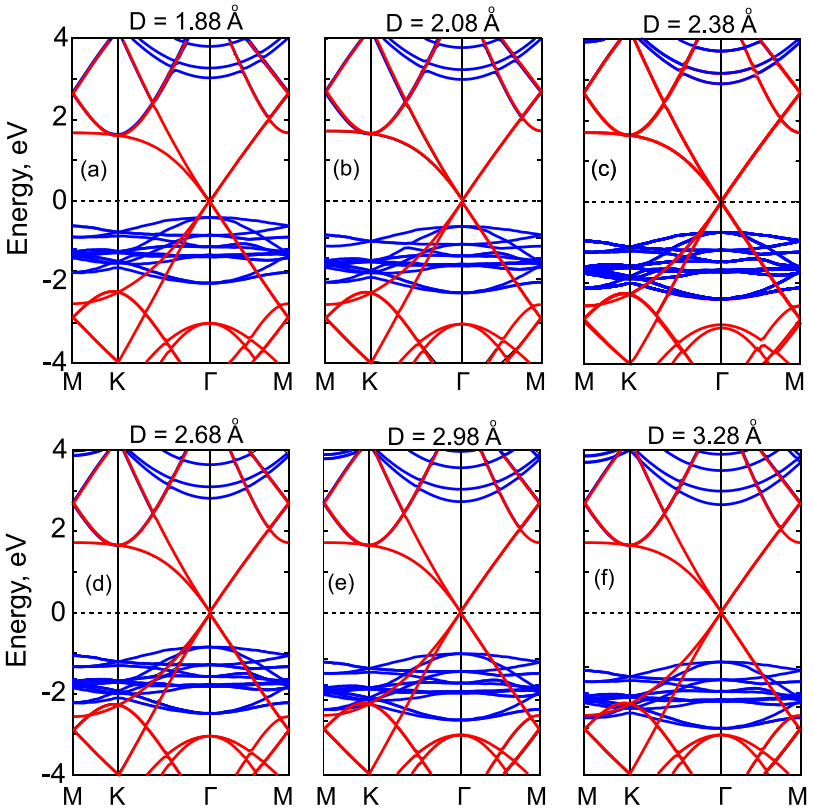

Fig. 7. Projected electronic band structures of the G/$Ca(OH)_2$ vdWH under different interlayer distances D_1, ranging from (a) D_1 = 1.88 Å, (b) D_1 = 2.08 Å, (c) D_1 = 2.38 Å, (d) D_1 = 2.68 Å, (e) D_1 = 2.98 AA, and D_1 = 3.28 Å, respectively.

field. The $\Phi_{B,n}$ is known to be more sensitive to the positive $E_\perp$, thus it decreases faster than the $\Phi_{B,p}$. Under the $E_\perp$ = +0.35 V/Å, the $\Phi_{B,n}$ continuously reduces and becomes smaller than the $\Phi_{B,p}$, indicating a transformation from the *p*SC-type to the *n*SC-type. Thus, it can be conclude that the positive $E_\perp$ can be used to modulate the Schottky barriers of the G/$Ca(OH)_2$ vdWH from the *p*SC-type to the *n*SC-type. The projected electronic band structures of the G/$Ca(OH)_2$ vdWH under positive $E_\perp$ are illustrated in Fig. 5(e-h). It is obvious that when the positive $E_\perp$ is introduced, there occurs the shift of the Fermi level of the G/$Ca(OH)_2$ vdWH from the VBM to the CBM of the semiconducting $Ca(OH)_2$ part. The $\Phi_{B,n}$ therefore, decreases gradually, whereas the $\Phi_{B,p}$ increases accordingly to the enlargement of the positive $E_\perp$ from 0 V/Å to +0.4 V/Å. When the positive $E_\perp \geq$ +0.35 VÅ, there occurs a transition from the *p*SC-type to the *n*SC-type of the G/$Ca(OH)_2$ vdWH. Therefore, these above results demonstrate that both the Schottky barriers and Schottky contact type of the G/$Ca(OH)_2$ vdWH can be turned effectively by applying electric field. Moreover, it should be noted that the electric field of $E_\perp$ = 0.4 V/Å can be realized in experiments by using the pulsed ac field technology [48]. Owing to these above promising properties, the G/$Ca(OH)_2$ vdWH is desirable material for designing high-performance Schottky devices.

Furthermore, the strain engineering is known to be an effective approach that widely used to modulate effectively the electronic properties of graphene-based vdWHs, such as G/SnS [49], G/$MoSe_2$ [50], G/GaN [44]. For instance, Xiong et al. [49] demonstrated that the electronic properties and the Schottky contact of the G/SnS vdWH are very sensitive to the strain engineering, which can be used to tune a transformation from the Schottky to the Ohmic contact. Sun et al. [44] showed a transition from the *n*SC-type to the *p*SC-type in the G/GaN vdWH by decreasing the interlayer coupling. In addition, the interlayer coupling D_1 in the vdWHs can be controlled experimentally by nanomechanical pressure [51] or by insertion of the dielectric layers [52]. Therefore, we further examine the influence of the strain engineering on the electronic properties and Schottky barrier of the G/$Ca(OH)_2$ vdWH. The strain engineering is applied to the G/$Ca(OH)_2$ vdWH along the *z* direction by changing the interlayer distance D_1, as shown in Fig. 6(a). We find that the $\Phi_{B,n}$ of the G/$Ca(OH)_2$ vdWH linearly decreases with increasing D_1, while the $\Phi_{B,p}$ linearly increases, as clearly shown in Fig. 6(b). When the D_1 increases from 1.88 Å to 2.38 Å and to 3.28 Å, the $\Phi_{B,n}$ decreases from 3.03 eV to 2.90 eV and to 2.66 eV, respectively, whereas the $\Phi_{B,p}$ increases from 0.70 eV to 0.78 eV and to 0.89 eV, respectively. However, the $\Phi_{B,n}$ is still larger than the $\Phi_{B,p}$ in the case of the enlargement of the D_1. Thus, the *p*SC-type is maintained in the G/$Ca(OH)_2$ vdWH. The projected electronic band structures of the G/$Ca(OH)_2$ vdWH illustrated in Fig. 7 show the influences of the strain engineering. When the D_1 is decreased from 2.38 Å down to 1.88 Å, the position of the Fermi level downshifts from the CBM to the VBM of the $Ca(OH)_2$ semiconductor. It leads to the gradual decrease (increase) in the $\Phi_{B,p}$ ($\Phi_{B,n}$). Quite the contrary, when the D_1 is increased the Fermi level moves upwards from the VBM to the CBM of the semiconductor $Ca(OH)_2$, leading to the gradual

increase (decrease) in the $\Phi_{B,p}$ ($\Phi_{B,n}$). The influences of the interlayer distance D_1 on the Schottky barriers of the G/$Ca(OH)_2$ vdWH can be explained as follows. As is well known that a potential step ΔV depends strongly on the strength of the charge transfer in the G/$Ca(OH)_2$ vdWH. When the charge transfer is enhanced, the potential step ΔV also becomes larger. Thus, when the D_1 is decreased, the charge transfer between the graphene and $Ca(OH)_2$ layer enhances, leading to an increase in the ΔV. Accordingly to the Eqs. (2) and (3), one can observe that the gradual increase in the ΔV results in the decrease/increase in the $\Phi_{B,p}/\Phi_{B,n}$. On the contrary, when the D_1 is increased, the charge transfer in the G/$Ca(OH)_2$ is weakened and the ΔV is reduced, leading to the increase/decrease in the $\Phi_{B,p}/\Phi_{B,n}$. Our results from Bader analysis demonstrate that when D was decreased from 3.28 Å to 1.88 Å, more electrons 0.0024, 0.004, 0.012 e for D = 3.28, D = 2.38 Å and D = 1.88 Å, respectively are transferred from graphene to $Ca(OH)_2$ layer.

4. Conclusion

In conclusion, in the framework of first principles calculations, we first proposed an ultrathin G/$Ca(OH)_2$ vdWH and then investigated comprehensively its electronic structures at the equilibrium state. The G/$Ca(OH)_2$ vdWH is mainly characterized by the physicoadsorption interaction with the interlayer distance of 2.38 Å and the binding energy of −33.37 meV/C atom. Interestingly, we found the formation of a small band gap of 9.7 meV opening at the Dirac point of G/$Ca(OH)_2$ vdWH, making it suitable for high speed electronic devices. The small carrier effective mass also reveals that the G/$Ca(OH)_2$ vdWH will exhibit high carrier mobility. Moreover, at the equilibrium state, such vdWH represents the pSC-type with small $\Phi_{B,p}$ = 0.78 eV, which can be tuned by strain engineering and electric field. The pSC-type is found to transformed to the nSC-type and then to OC-type when a negative electric field is larger than −0.3 V/Å. Our results demonstrate a useful of the G/$Ca(OH)_2$ vdWH towards electronic and optoelectronic applications and a route to improve these devices performance based on such heterostructure, such as Schottky devices.

References

[1] K.S. Novoselov, A.K. Geim, S.V. Morozov, D. Jiang, Y. Zhang, S.V. Dubonos, I.V. Grigorieva, A.A. Firsov, Electric field effect in atomically thin carbon films, Science 306 (5696) (2004) 666–669.

[2] Y.-M. Lin, C. Dimitrakopoulos, K.A. Jenkins, D.B. Farmer, H.-Y. Chiu, A. Grill, P. Avouris, 100-ghz transistors from wafer-scale epitaxial graphene, Science 327 (5966) (2010) 662.

[3] M.C. Lemme, T.J. Echtermeyer, M. Baus, H. Kurz, A graphene field-effect device, IEEE Electron Device Lett. 28 (4) (2007) 282–284.

[4] F. Xia, T. Mueller, Y.-m. Lin, A. Valdes-Garcia, P. Avouris, Ultrafast graphene photodetector, Nat. Nanotechnol. 4 (12) (2009) 839.

[5] K.S. Novoselov, A.K. Geim, S. Morozov, D. Jiang, M. Katsnelson, I. Grigorieva, S. Dubonos, A. Firsov, Two-dimensional gas of massless dirac fermions in graphene, Nature 438 (7065) (2005) 197.

[6] Y. Liu, Z.-Y. Ong, J. Wu, Y. Zhao, K. Watanabe, T. Taniguchi, D. Chi, G. Zhang, J.T. Thong, C.-W. Qiu, et al., Thermal conductance of the 2D MoS_2/h-BN and graphene/h-BN interfaces, Sci. Rep. 7 (2017) 43886.

[7] Z.-Y. Ong, G. Zhang, Y.-W. Zhang, Controlling the thermal conductance of graphene/h- BN lateral interface with strain and structure engineering, Phys. Rev. B 93 (7) (2016) 075406.

[8] V.H. Nguyen, F. Mazzamuto, A. Bournel, P. Dollfus, Resonant tunnelling diodes based on graphene/h-BN heterostructure, J. Phys. D: Appl. Phys. 45 (32) (2012) 325104.

[9] C.R. Dean, A.F. Young, I. Meric, C. Lee, L. Wang, S. Sorgenfrei, K. Watanabe, T. Taniguchi, P. Kim, K.L. Shepard, et al., Boron nitride substrates for high-quality graphene electronics, Nat. Nanotechnol. 5 (10) (2010) 722.

[10] W. Kim, C. Li, F.A. Chaves, D. Jiménez, R.D. Rodriguez, J. Susoma, M.A. Fenner, H. Lipsanen, J. Riikonen, Tunable graphene–GaSe dual heterojunction device, Adv. Mater. 28 (9) (2016) 1845–1852.

[11] Z. Ben Aziza, H. Henck, D. Pierucci, M.G. Silly, E. Lhuillier, G. Patriarche, F. Sirotti, M. Eddrief, A. Ouerghi, Van der waals epitaxy of GaSe/graphene heterostructure: electronic and interfacial properties, ACS Nano 10 (10) (2016) 9679–9686.

[12] Z.B. Aziza, D. Pierucci, H. Henck, M.G. Silly, C. David, M. Yoon, F. Sirotti, K. Xiao, M. Eddrief, J.-C. Girard, et al., Tunable quasiparticle band gap in few-layer GaSe/graphene van der waals heterostructures, Phys. Rev. B 96 (3) (2017) 035407.

[13] C. Si, Z. Lin, J. Zhou, Z. Sun, Controllable schottky barrier in GaSe/graphene heterostructure: the role of interface dipole, 2D Mater. 4 (1) (2016) 015027.

[14] S. Sattar, U. Schwingenschlögl, Electronic properties of graphene–$PtSe_2$ contacts, ACS Appl. Mater. Interfaces 9 (18) (2017) 15809–15813.

[15] Z. Guan, S. Ni, S. Hu, Band gap opening of graphene by forming a graphene/$PtSe_2$ van der waals heterojunction, RSC Adv. 7 (72) (2017) 45393–45399.

[16] C. Xia, J. Du, L. Fang, X. Li, X. Zhao, X. Song, T. Wang, J. Li, $PtSe_2$/graphene hetero-multilayer: gate-tunable schottky barrier height and contact type, Nanotechnology 29 (46) (2018) 465707.

[17] M. Sun, J.-P. Chou, J. Yu, W. Tang, Effects of structural imperfection on the electronic properties of graphene/WSe_2 heterostructures, J. Mater. Chem. C 5 (39) (2017) 10383–10390.

[18] H.-L. Tang, M.-H. Chiu, C.-C. Tseng, S.-H. Yang, K.-J. Hou, S.-Y. Wei, J.-K. Huang, Y.-F. Lin, C.-H. Lien, L.-J. Li, Multilayer Graphene–WSe_2 heterostructures for WSe_2 transistors, ACS Nano 11 (12) (2017) 12817–12823.

[19] B. Yang, M. Lohmann, D. Barroso, I. Liao, Z. Lin, Y. Liu, L. Bartels, K. Watanabe, T. Taniguchi, J. Shi, Strong electron–hole symmetric rashba spin–orbit coupling in graphene/monolayer transition metal dichalcogenide heterostructures, Phys. Rev. B 96 (2017) 041409.

[20] Y. Cai, G. Zhang, Y.-W. Zhang, Electronic properties of phosphorene/graphene and phosphorene/hexagonal boron nitride heterostructures, J. Phys. Chem. C 119 (24) (2015) 13929–13936.

[21] B. Liu, L.-J. Wu, Y.-Q. Zhao, L.-Z. Wang, M.-Q. Cai, Tuning the schottky contacts in the phosphorene and graphene heterostructure by applying strain, Phys. Chem. Chem. Phys. 18 (29) (2016) 19918–19925.

[22] M. Sun, J.-P. Chou, J. Yu, W. Tang, Electronic properties of blue phosphorene/graphene and blue phosphorene/graphene-like gallium nitride heterostructures, Phys. Chem. Chem. Phys. 19 (26) (2017) 17324–17330.

[23] Y.-T. Du, X. Kan, F. Yang, L.-Y. Gan, U. Schwingenschlögl, Mxene/graphene heterostructures as high-performance electrodes for li-ion batteries, ACS Appl. Mater. Interfaces 10 (38) (2018) 32867–32873.

[24] S. Zhou, X. Yang, W. Pei, N. Liu, J. Zhao, Heterostructures of MXenes and N-doped graphene as highly active bifunctional electrocatalysts, Nanoscale 10 (23) (2018) 10876–10883.

[25] R. Li, W. Sun, C. Zhan, P.R.C. Kent, D.-e. Jiang, Interfacial and electronic properties of heterostructures of MXene and graphene, Phys. Rev. B 99 (2019) 085429.

[26] S. Wang, J.-P. Chou, C. Ren, H. Tian, J. Yu, C. Sun, Y. Xu, M. Sun, Tunable schottky barrier in graphene/graphene-like germanium carbide van der waals heterostructure, Sci. Rep. 9 (1) (2019) 5208.
[27] Y. Aierken, H. Sahin, F. Iyikanat, S. Horzum, A. Suslu, B. Chen, R.T. Senger, S. Tongay, F.M. Peeters, Portlandite crystal: Bulk, bilayer, and monolayer structures, Phys. Rev. B 91 (24) (2015) 245413.
[28] C. Xia, W. Xiong, J. Du, T. Wang, Z. Wei, J. Li, Robust electronic and mechanical properties to layer number in 2D wide-gap $X(OH)_2$ (X= Mg, Ca), J. Phys. D: Appl. Phys. 51 (1) (2017) 015107.
[29] C. Xia, W. Xiong, J. Du, Y. Peng, Z. Wei, J. Li, Electric field modulations of band alignments in arsenene/Ca $(OH)_2$ heterobilayers for multi-functional device applications, J. Phys. D: Appl. Phys. 50 (41) (2017) 415304.
[30] C. Bacaksiz, A. Dominguez, A. Rubio, R.T. Senger, H. Sahin, H-AlN-$Mg(OH)_2$ van der waals bilayer heterostructure: Tuning the excitonic characteristics, Phys. Rev. B 95 (7) (2017) 075423.
[31] Q. Gao, C. Xia, W. Xiong, J. Du, T. Wang, Z. Wei, J. Li, Type-i $Ca(OH)_2/\alpha$-$MoTe_2$ vdw heterostructure for ultraviolet optoelectronic device applications: electric field effects, J. Mater. Chem. C 5 (47) (2017) 12629–12634.
[32] E. Torun, H. Sahin, F. Peeters, Optical properties of GaS-$Ca(OH)_2$ bilayer heterostructure, Phys. Rev. B 93 (7) (2016) 075111.
[33] P. Giannozzi, S. Baroni, N. Bonini, M. Calandra, R. Car, C. Cavazzoni, D. Ceresoli, G.L. Chiarotti, M. Cococcioni, I. Dabo, et al., Quantum espresso: a modular and open-source software project for quantum simulations of materials, J. Phys. Condens. Matt. 21 (39) (2009) 395502.
[34] P.E. Blöchl, Projector augmented-wave method, Phys. Rev. B 50 (24) (1994) 17953.
[35] J. Perdew, K. Burke, M. Ernzerhof, Perdew, burke, and ernzerhof reply, Phys. Rev. Lett. 80 (4) (1998) 891.
[36] S. Grimme, Semiempirical gga-type density functional constructed with a long-range dispersion correction, J. Comput. Chem. 27 (15) (2006) 1787–1799.
[37] K.D. Pham, N.N. Hieu, H.V. Phuc, I. Fedorov, C. Duque, B. Amin, C.V. Nguyen, Layered graphene/GaS van der waals heterostructure: Controlling the electronic properties and schottky barrier by vertical strain, Appl. Phys. Lett. 113 (17) (2018) 171605.
[38] H.V. Phuc, N.N. Hieu, B.D. Hoi, C.V. Nguyen, Interlayer coupling and electric field tunable electronic properties and schottky barrier in a graphene/bilayer-gase van der waals heterostructure, Phys. Chem. Chem. Phys. 20 (26) (2018) 17899–17908.
[39] J. Heyd, G.E. Scuseria, M. Ernzerhof, Hybrid functionals based on a screened coulomb potential, J. Chem. Phys. 118 (18) (2003) 8207–8215.
[40] W. Tang, E. Sanville, G. Henkelman, A grid-based bader analysis algorithm without lattice bias, J. Phys.: Condens. Matter 21 (8) (2009) 084204.
[41] E. Sanville, S.D. Kenny, R. Smith, G. Henkelman, Improved grid-based algorithm for bader charge allocation, J. Comput. Chem. 28 (5) (2007) 899–908.
[42] G. Henkelman, A. Arnaldsson, H. Jónsson, A fast and robust algorithm for bader decomposition of charge density, Comput. Mater. Sci. 36 (3) (2006) 354–360.
[43] M. Yu, D.R. Trinkle, Accurate and efficient algorithm for bader charge integration, J. Chem. Phys. 134 (6) (2011) 064111.
[44] M. Sun, J.-P. Chou, Q. Ren, Y. Zhao, J. Yu, W. Tang, Tunable schottky barrier in van der waals heterostructures of graphene and g-GaN, Appl. Phys. Lett. 110 (17) (2017) 173105.
[45] K. Ren, M. Sun, Y. Luo, S. Wang, J. Yu, W. Tang, First-principle study of electronic and optical properties of two-dimensional materials-based heterostructures based on transition metal dichalcogenides and boron phosphide, Appl. Surf. Sci. 476 (2019) 70–75.
[46] Y. Luo, S. Wang, K. Ren, J.-P. Chou, J. Yu, Z. Sun, M. Sun, Transition-metal dichalcogenides/$Mg(OH)_2$ van der Waals heterostructures as promising water-splitting photocatalysts: a first-principles study, Phys. Chem. Chem. Phys. 21 (2019) 1791–1796.
[47] J. Bardeen, Surface states and rectification at a metal semi-conductor contact, Phys. Rev. 71 (10) (1947) 717.
[48] C. Vicario, B. Monoszlai, C.P. Hauri, GV/m Single-cycle terahertz fields from a laser-driven large-size partitioned organic crystal, Phys. Rev. Lett. 112 (2014) 213901.
[49] W. Xiong, C. Xia, X. Zhao, T. Wang, Y. Jia, Effects of strain and electric field on electronic structures and schottky barrier in graphene and SnS hybrid heterostructures, Carbon 109 (2016) 737–746.
[50] F. Zhang, W. Li, Y. Ma, X. Dai, Strain effects on the schottky contacts of graphene and $MoSe_2$ heterobilayers, Physica E 103 (2018) 284–288.
[51] M. Dienwiebel, G.S. Verhoeven, N. Pradeep, J.W. Frenken, J.A. Heimberg, H.W. Zandbergen, Superlubricity of graphite, Phys. Rev. Lett. 92 (12) (2004) 126101.
[52] H. Fang, C. Battaglia, C. Carraro, S. Nemsak, B. Ozdol, J.S. Kang, H.A. Bechtel, S.B. Desai, F. Kronast, A.A. Unal, G. Conti, C. Conlon, G.K. Palsson, M.C. Martin, A.M. Minor, C.S. Fadley, E. Yablonovitch, R. Maboudian, A. Javey, Strong interlayer coupling in van der waals heterostructures built from single-layer chalcogenides, Proc. Natl. Acad. Sci. USA 111 (17) (2014) 6198–6202.